Molecular Origins of Optoelectronic Properties in Coumarin Dyes: Toward Designer Solar Cell and Laser Applications

ARTICLE *in* THE JOURNAL OF PHYSICAL CHEMISTRY A · NOVEMBER 2011

Impact Factor: 2.69 · DOI: 10.1021/jp209925y · Source: PubMed

6 AUTHORS, INCLUDING:

Xiaogang Liu
Singapore-MIT Alliance for Research and Tec…
17 PUBLICATIONS **372** CITATIONS
SEE PROFILE

Tze-Chia Lin
University of Cambridge
8 PUBLICATIONS **101** CITATIONS
SEE PROFILE

Anita Zeidler
University of Bath
37 PUBLICATIONS **406** CITATIONS
SEE PROFILE

THE JOURNAL OF PHYSICAL CHEMISTRY A

ARTICLE

pubs.acs.org/JPCA

Molecular Origins of Optoelectronic Properties in Coumarin Dyes: Toward Designer Solar Cell and Laser Applications

Xiaogang Liu,[†] Jacqueline M. Cole,[*,†,‡,§,∥] Paul G. Waddell,[†,‡] Tze-Chia Lin,[†] Jignesh Radia,[†] and Anita Zeidler[∥,⊥]

[†]Cavendish Laboratory, Department of Physics, University of Cambridge, J. J. Thomson Avenue, Cambridge, CB3 0HE United Kingdom

[‡]Department of Chemistry, and [§]Department of Physics, University of New Brunswick, P.O. Box 4400, Fredericton, NB, E3B 5A3 Canada

[∥]Department of Chemistry, University of Cambridge, Lensfield Road, Cambridge, CB2 1EW United Kingdom

Supporting Information

ABSTRACT: Coumarin derivatives are used in a wide range of applications, such as dye-sensitized solar cells (DSCs) and dye lasers, and have therefore attracted considerable research interest. In order to understand the molecular origins of their optoelectronic properties, molecular structures for 29 coumarin laser dyes are statistically analyzed. To this end, data for 25 compounds were taken from the Cambridge Structural Database and compared with data for four new crystal structures of coumarin laser dyes [Coumarin 487 ($C_{19}H_{23}NO_2$), Coumarin 498 ($C_{16}H_{17}NO_4S$), Coumarin 510 ($C_{20}H_{18}N_2O_2$), and Coumarin 525 ($C_{22}H_{18}N_2O_3$)], which are reported herein. The competing contributions of different resonance states to the bond lengths of the 4- and 7-substituted coumarin laser dyes are computed based on the harmonic oscillator stabilization energy model. Consequently, a positive correlation between the contribution of the *para*-quinoidal resonance state and the UV−vis peak absorption wavelength of these coumarins is revealed. Furthermore, the perturbations of optoelectronic properties, owing to chemical substituents in these coumarin laser dyes, are analyzed: it is found that their UV−vis peak absorption and lasing wavelengths experience a red shift, as the electron-donating strength of the 7-position substituent increases and/or the electron-withdrawing strength of the 3- or 4-position substituent rises; this conclusion is corroborated by quantum-chemical calculations. It is also revealed that the closer the relevant substituents align with the direction of the intramolecular charge transfer (ICT), the larger the spectral shifts and the higher the molar extinction coefficients of coumarin laser dyes. These findings are important for understanding the ICT mechanism in coumarins. Meanwhile, all structure−property correlations revealed herein will enable knowledge-based molecular design of coumarins for dye lasers and DSC applications.

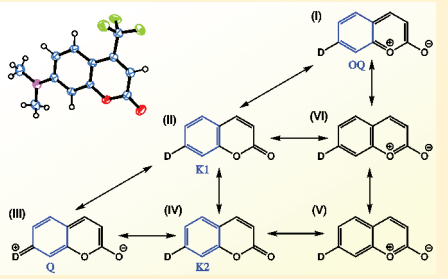

1. INTRODUCTION

Coumarin (2H-chromen-2-one) and its derivatives have attracted substantial interest in a wide range of research areas, from their key role in pharmaceutical agents, such as anti-inflammatory and antioxidant agents,[1] HIV inhibitors,[2] and anticoagulants,[3] to their widespread industrial use as dye lasers.[4] In recent years, there has also been a drive to synthesize coumarin-based organic dyes for use in high-efficiency dye-sensitized solar cells (DSCs).[5,6] In order to facilitate this synthesis, this paper investigates the molecular origins of the functional optoelectronic properties that make coumarins so attractive. Thereupon, one can establish the molecular building blocks that are required to design higher-performance coumarin dyes.

This study focuses on the bond-length patterns of 29 coumarin-based commercial laser dyes (Scheme 1), based on data taken from the Cambridge Structural Database (CSD)[7] and our own single-crystal X-ray diffraction (XRD) experiments. The aim is to reveal relationships between these molecular structures and their optoelectronic properties; specifically their light absorption characteristics, with a view to using these relationships to design more efficient coumarins for DSC applications.

Coumarin is a molecule consisting of a benzene ring fused together with a lactone ring. The lactone ring also contains a double bond such that it extends the conjugated π-system across the molecule. A schematic drawing of the coumarin molecular structure, together with its position-numbering convention and atomic labeling used in this paper, is shown in Figure 1. In addition, we define the aromatic ring consisting of 6 carbon atoms as ring 1 and the lactone ring as ring 2. Henceforth, the name, coumarin, will refer to both coumarin itself (2H-chromen-2-one) and its coumarin-based derivatives.

Common to all coumarin-based laser dyes under discussion is an electron-donating substituent attached at the 7-position (most commonly an amine group). In these dyes, intramolecular

Received: October 15, 2011
Revised: November 24, 2011
Published: November 28, 2011

Scheme 1. Molecular Structures of Selected Coumarin Laser Dyes[a]

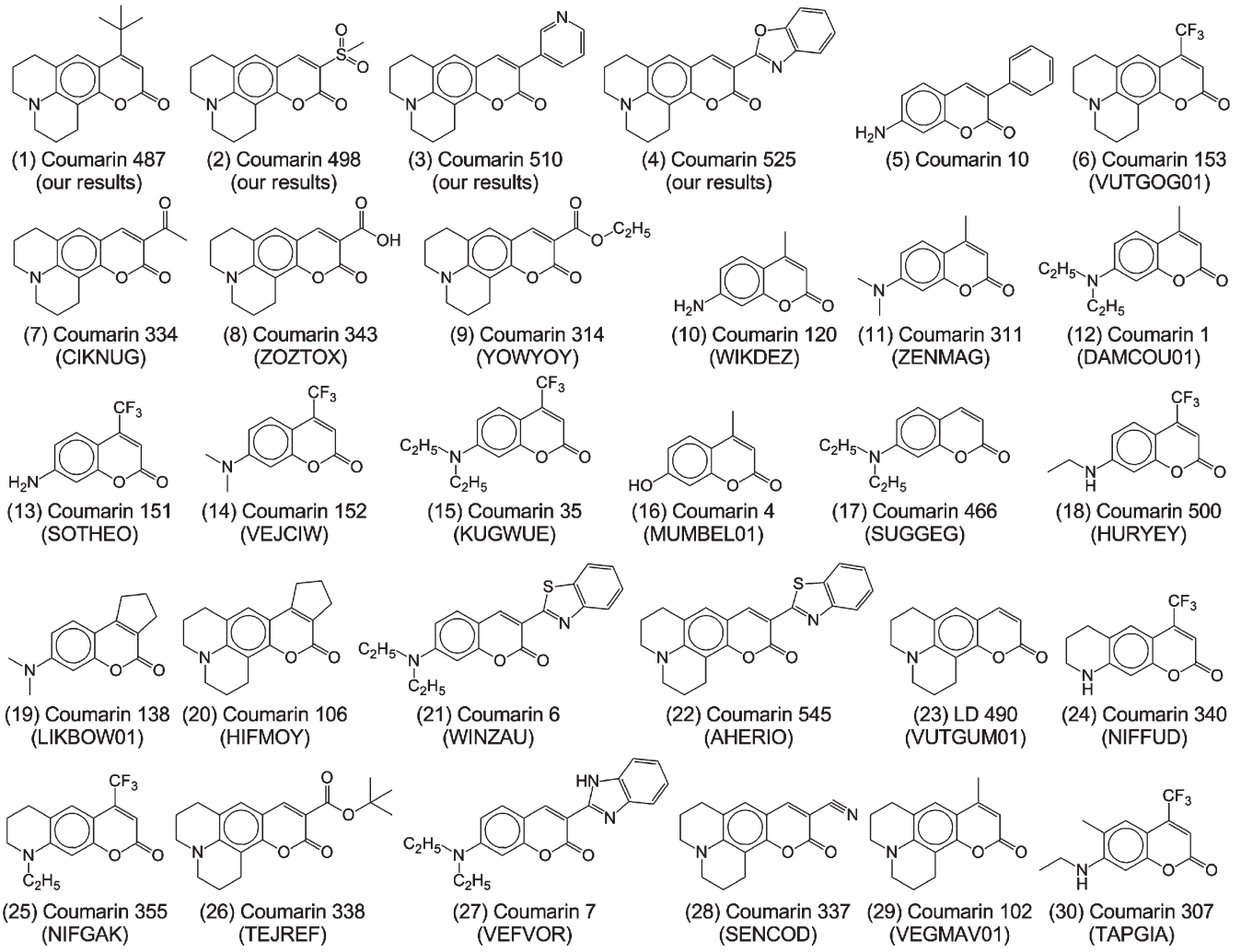

[a] The crystal structures of **1**−**4** are determined from our own XRD experiments, while those of **6**−**30** with their CSD reference codes are enclosed in brackets. The crystal structure of **5** has not been reported, to date; however, its molar extinction coefficient is analyzed in this study and its chemical schematic representation is presented here as well. Consequently, there are 29 sets of coumarin crystal structural data in total.

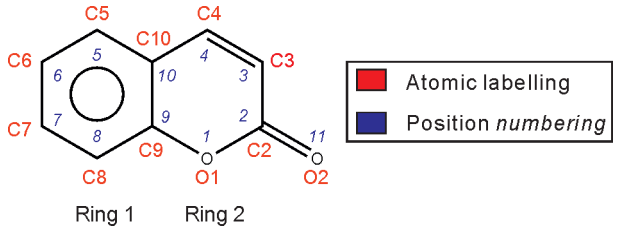

Figure 1. Molecular structure of coumarin and its atomic and ring labeling and position numbering designations.

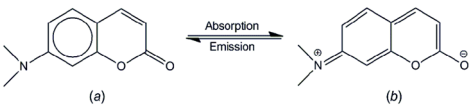

Figure 2. Intramolecular charge transfer (ICT) in 7-dimethylamino-coumarin via absorption and emission. Aromatic ring 1 in (a) becomes *para*-quinoidal in (b) upon photo excitation.

charge transfer (ICT) occurs when they are excited via light absorption (Figure 2).[4] The ICT process can be assisted by this electron-donating group at the 7-position and/or an electron-withdrawing group either at the 3- or 4-position via resonance and inductive effects. This "push-pull" effect on the electronic charge perturbs the aromatic nature of ring 1 in resonance state, Figure 2a, toward a *para*-quinoidal structural configuration, Figure 2b, even in the absence of light excitation. In this *para*-quinoidal resonance state, bonds C5−C6 and C8−C9, which are parallel to each other, are more akin to a double bond, whereas the remaining four carbon bonds in ring 1 are more representative of a single bond. Due to the competing contribution of this resonance state, bonds C5−C6 and C8−C9 become shorter when compared to neighboring carbon bonds. Such molecular structures have been reported for a few 7-hydroxycoumarins.[8]

We herein show that resonance theory and the "push-pull" effect can be used to explain the bond-length patterns in coumarins as well as their optoelectronic properties, with specific

Table 1. XRD Experimental Details

	1 Coumarin 487	**2** Coumarin 498	**3** Coumarin 510	**4** Coumarin 525
chemical formula	$C_{19}H_{23}NO_2$	$C_{16}H_{17}NO_4S$	$C_{20}H_{18}N_2O_2$	$C_{22}H_{18}N_2O_3$
M_r	297.38	319.37	318.36	358.38
crystal system, space group	monoclinic, $P2_1/c$	monoclinic, $P2_1/c$	monoclinic, $P2_1/c$	monoclinic, $P2_1/c$
temperature (K)	150	180	120	180
a, b, c (Å)	22.261 (9), 7.709 (3), 20.227 (8)	11.466 (2), 15.725 (3), 18.776 (6)	11.4302 (8), 13.0417 (9), 10.2164 (7)	13.1252 (4), 7.3464 (2), 17.3911 (7)
β (°)	116.454 (4)	119.73 (2)	92.823 (3)	97.2558 (12)
V (Å^3)	3108 (2)	2939.8 (12)	1521.10 (18)	1663.47 (10)
Z	8	8	4	4
μ (mm^{-1})	0.08	0.24	0.09	0.10
T_{min}, T_{max}	0.961, 0.969	0.932, 0.967	0.985, 0.991	0.933, 0.993
no. of measured, independent and observed [$I > 2\sigma(I)$] reflections	10953, 6986, 4218	19809, 6697, 4530	10914, 3248, 2009	8478, 3580, 2582
R_{int}	0.052	0.054	0.083	0.042
$R[F^2 > 2\sigma(F^2)]$, $wR(F^2)$, S	0.052, 0.136, 0.92	0.052, 0.124, 1.06	0.055, 0.154, 0.91	0.053, 0.136, 1.02
no. of reflections	6986	6697	3248	3580
no. of parameters	581	399	217	251
$\Delta\rho_{max}$, $\Delta\rho_{min}$ (e Å^{-3})	0.26, −0.28	0.37, −0.50	0.36, −0.29	0.25, −0.22

reference to their absorption wavelengths and molar extinction coefficients. It will be shown that the *para*-quinoidal configuration is not exclusive to 7-hydroxycoumarins but is observed in a wide range of laser dye coumarins as a result of the ICT. Furthermore, as the "push-pull" effect becomes stronger, the contribution of the *para*-quinoidal resonance state increases; in turn, this enhances the red shift in the UV−vis peak absorption wavelengths of these coumarins. In particular for coumarins with substituents only at the 7- and/or 4-position(s), an approximately *linear* relationship between the *para*-quinoidal state contribution and the red shift is observed, since the "push-pull" effect occurs *nearly* along the *para*-direction from C7 to C10 in ring 1. As an electron-withdrawing substituent moves from the 4- to the 3-position, the resulting "push-pull" effect aligns more closely with the direction of the ICT from the 7-position to O2. The red shift of the absorption wavelength is even more pronounced in such a coumarin dye, whereas an enhancement of the molar extinction coefficient is also observed.

2. EXPERIMENTAL SECTION

2.1. X-ray Diffraction Experiments. As the structural data of many coumarins are not available, we augmented our statistical survey by determining crystal structures of four compounds: Coumarin 487 ($C_{19}H_{23}NO_2$; **1**); Coumarin 498 ($C_{16}H_{17}NO_4S$; **2**); Coumarin 510 ($C_{20}H_{18}N_2O_2$; **3**); and Coumarin 525 ($C_{22}H_{18}N_2O_3$; **4**) (Scheme 1).

These compounds were supplied by the Exciton chemical company. Crystals of **1** suitable for single crystal X-ray diffraction were grown via slow diffusion of diethyl ether into a solution of the compound in dichloromethane at room temperature. Crystals of the remaining compounds were grown via slow solvent evaporation in methanol at room temperature.

For **1** and **3**, data were collected at 150 and 120 K, respectively, on a Rigaku Saturn 724+ CCD diffractometer equipped with a molybdenum X-ray source ($\lambda_{MoK\alpha}$ = 0.71073 Å) and accompanying SHINE Optics. An open-flow nitrogen Oxford Cryosystems CryostreamPlus was used to cool the sample. Rigaku *CrystalClear*-SM Expert 2.0 software was used for all data collection, cell refinement and data reduction procedures.[9]

For **2** and **4**, data were collected at 180 K on a Nonius KappaCCD area-detector diffractometer equipped with a Mo Kα X-ray source and an open-flow nitrogen Oxford Cryosystems Cryostream. Data collection employed the software *COLLECT*;[10] cell refinement and data reduction were conducted using software *HKL DENZO* and *SCALEPACK*.[11]

For all four compounds, data were corrected for absorption effects by comparing equivalent reflections with SORTAV;[12] SHELXS97[13] and SHELXL97[13] were used, respectively, to solve and refine the structures. Hydrogen atoms were refined as follows: for **1**, all hydrogen atoms were located from the difference map of electron density and their coordinates were refined freely; for the remaining compounds, all hydrogen atoms were positioned geometrically and refined as riding on their parent atoms, with C—H = 0.980 Å and $U_{iso}(H) = 1.5U_{eq}(C)$ for methyl H atoms, C—H = 0.950 Å and $U_{iso}(H) = 1.2U_{eq}(C)$ for aromatic H atoms, and C—H = 0.990 Å and $U_{iso}(H) = 1.2U_{eq}(C)$ for other types of hydrogen atoms.

ORTEP-3 for Windows[14] was employed in order to prepare molecular graphics while publCIF[15] was executed for preparing publication material.

A summary of crystal, data collection and refinement details is given in Table 1.

2.2. Preparation of Laser Dye Bond Length, Wavelength, and Molar Extinction Coefficient Data. A list of coumarin laser dyes was compiled based on the product catalogues from two major suppliers, Exciton and Lambda Physik, as well as existing literature on laser dyes that originated mainly from Eastman Kodak and the Naval Weapons Center (U.S.A.; Supporting Information). Crystal structures of the coumarins in this list were sought via the CSD. A CSD-generated reference code uniquely identifies each database entry of a crystal structure. This takes the form of a six-letter code unless there are duplicate database entries of the same chemical compound; in that event, two digits extend this code to rank the chronological order of duplicate presentations. This paper uses this reference code to identify

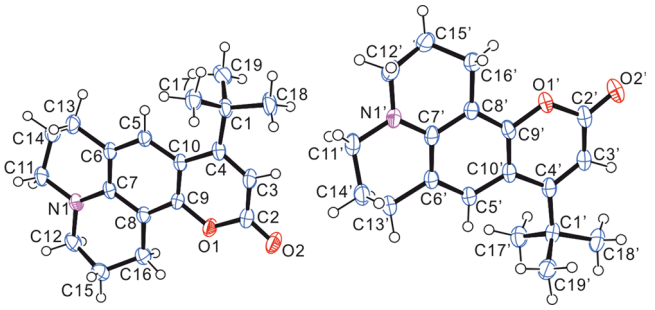

Figure 3. Crystallographic asymmetric unit of **1** at 150 K with anisotropic displacement ellipsoids drawn at the 50% probability level.

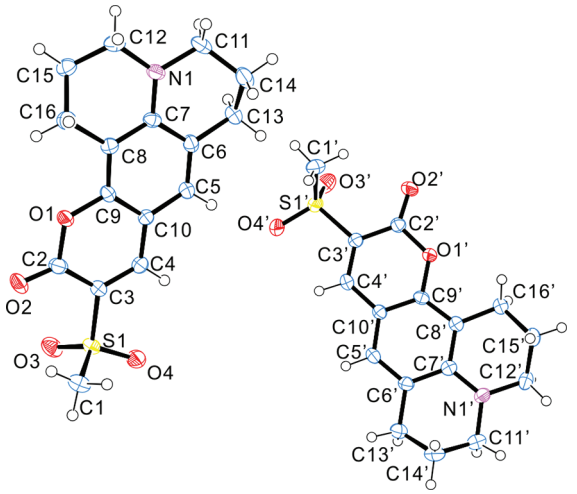

Figure 4. Crystallographic asymmetric unit of **2** at 180 K with anisotropic displacement ellipsoids drawn at the 50% probability level.

crystal structural data exported from the CSD. Where structural data for a given coumarin was not available from the CSD, our experimental results derived the bond geometries. The UV−vis peak absorption and lasing wavelengths of these coumarins were also tabulated as reported by the relevant product datasheet or literature.

Certain reports of UV−vis peak absorption and lasing wavelength values for a given laser dye were at slight variance. In such cases, a single value was extracted from duplicate data using the following selection criteria: (i) If the values available are quite close to each other (within 5 nm), the average value is taken, and this value is rounded off to an integer and given in nm. (ii) If the deviation for a given laser dye is large (>5 nm), the most credible value to the best of our knowledge is selected.

Molar extinction coefficients (ε) for 23 laser dye coumarins were imported from the literature.[16,17] There were small differences in ε values between the two sources for several coumarins; however, such errors were generally negligible. In cases of discrepancy, the data of Reynolds and Drexhage[16] were cited, as the majority of data were drawn from this reference and so this selection ensured the same experimental conditions for most of these coumarins.

Full tables of coumarin laser dyes with their CSD reference codes, bond lengths, spectral information, and molar extinction coefficients are deposited in the Supporting Information.

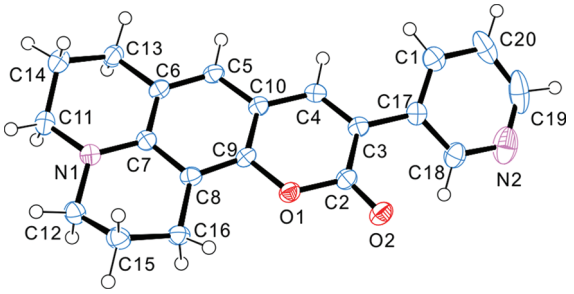

Figure 5. Crystallographic asymmetric unit of **3** at 120 K with anisotropic displacement ellipsoids drawn at the 50% probability level.

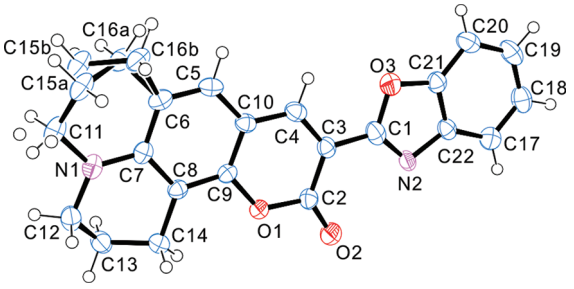

Figure 6. Crystallographic asymmetric unit of **4** at 180 K with anisotropic displacement ellipsoids drawn at the 50% probability level. There are two atoms, C15 and C16, which are disordered with relative occupancies of 85.5(4)%:14.5(4)%.

2.3. Quantum-Chemical Calculations. Quantum-chemical calculations were performed on Coumarin 120 ($C_{10}H_9NO_2$; **10**), Coumarin 311 ($C_{12}H_{13}NO_2$; **11**), Coumarin 1 ($C_{14}H_{17}NO_2$; **12**), Coumarin 151 ($C_{10}H_6F_3NO_2$; **13**), Coumarin 152 ($C_{12}H_{10}F_3NO_2$; **14**), and Coumarin 35 ($C_{14}H_{14}F_3NO_2$; **15**) (Scheme 1) using *Gaussian 09*.[18] This enabled a comparison of bandgaps and the nature of electronic charge transfer upon photoexcitation in these compounds to be studied.

The geometries of these molecules were optimized with density functional theory (DFT) using Becke's three-parameter and Lee−Yang−Parr functional[19−21] (B3LYP) and a 6-31G(d) basis set.[22] Subsequent frequency checks showed that minima on their respective potential energy surfaces were obtained. The highest occupied molecular orbitals (HOMOs) and lowest unoccupied molecular orbitals (LUMOs) of these coumarins were calculated with DFT using the hybrid B3LYP functional and a 6-31++G(d,p) basis set,[22] based on the optimized molecular structures.

In addition, single-point energy calculations were performed with *Gaussian 09* using the B3LYP functional and the 6-31++G(d,p) basis set on two different sets of structural data for **14**. This extra calculation was needed because the crystal structure of this compound is reported in the CSD[7] in two different polymorphs, *Pnma* for VEJCIW[23] and $P2_1/a$ for VEJCIW01,[24] both at room temperature; the most thermodynamically stable compound (VEJCIW) needed to be determined.

3. RESULTS AND DISCUSSION

3.1. Four New Crystal Structures of Coumarins: 1−4. 50% probability anisotropic displacement ellipsoidal plots for **1**−**4** are given in Figures 3−6, respectively. Selected bond lengths and torsion angles for these compounds are available in Table 2,

Table 2. Selected Bond Lengths and Torsion Angles of the Four New Coumarin Laser Dye Crystal Structures Reported Herein[a]

	1 Coumarin 487		2 Coumarin 498			
	molecule 1	molecule 2	molecule 1	molecule 2	3 Coumarin 510	4 Coumarin 525
			Bond Lengths (Å)			
C6−C7	1.416(2)	1.416(2)	1.441(3)	1.437(3)	1.430(3)	1.433(3)
C7−C8	1.415(2)	1.411(2)	1.420(3)	1.415(3)	1.418(3)	1.419(2)
C8−C9	1.389(2)	1.388(2)	1.378(3)	1.381(3)	1.382(3)	1.380(3)
C9−C10	1.402(2)	1.406(2)	1.411(3)	1.402(3)	1.399(3)	1.403(2)
C5−C10	1.414(2)	1.422(2)	1.410(3)	1.405(3)	1.405(3)	1.409(3)
C5−C6	1.375(2)	1.381(2)	1.364(3)	1.366(3)	1.367(3)	1.365(3)
C9−O1	1.384 (2)	1.387(2)	1.384(2)	1.385(2)	1.382(2)	1.378(2)
C2−O1	1.376(2)	1.377(2)	1.390(3)	1.385(3)	1.382(2)	1.398(2)
C2−C3	1.435(3)	1.433(3)	1.442(3)	1.438(3)	1.460(3)	1.451(3)
C3−C4	1.361(2)	1.361(2)	1.368(3)	1.363(3)	1.360(3)	1.369(3)
C4−C10	1.455(2)	1.455(2)	1.404(3)	1.412(3)	1.421(3)	1.402(3)
C2−O2	1.216(2)	1.218(2)	1.203(3)	1.211(3)	1.210(2)	1.205(2)
C7−N1	1.368(2)	1.369(2)	1.355(3)	1.364(3)	1.381(2)	1.361(2)
			Torsion Angles (deg)			
C6−C7−N1−C11	5.4(3)	6.7(2)	−12.8(3)	1.3(3)	10.5(3)	−7.2(3)
C8−C7−N1−C12	5.0(3)	6.3(3)	−5.8(3)	−9.6(3)	−13.7(3)	−5.0(3)
χ_N	0.4(4)	0.4(4)	6.7(4)	10.9(4)	24.2(4)	2.2(4)

[a] χ_N denotes the absolute value of the difference between the two torsion angles along C7−N1. This angle represents the overall out-of-plane torsion angle of the two substituent branches attached to the N1 atom with respect to the ring 1 plane in a coumarin.

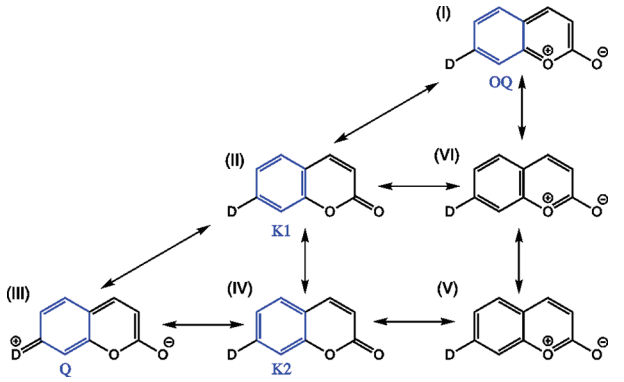

Figure 7. Possible resonance structures in coumarin laser dyes. Although only the 7-position electron-donating substituent, D, is shown here, other substituents are likely to be attached onto this framework. The blue-highlighted ring 1 moieties represent four distinct canonical molecular fragments: Q (*para*-quinoidal), OQ (*ortho*-quinoidal), K1 (Kekulé configuration 1), and K2 (Kekulé configuration 2). Their relative contributions toward the overall XRD-derived structure of ring 1 can be quantified by the harmonic oscillator stabilization energy (HOSE) model (see section 3.4).

whereas full structural data for all four coumarins can be found in the Supporting Information.

3.2. Possible Resonance States in Coumarins. Resonance theory can be used to elucidate structural patterns in π-conjugated organic molecules.[25−27] By applying this theory, all possible resonance structures (canonical forms) of a π-conjugated molecule can be identified. By comparing these canonical forms with the molecular structure obtained from an XRD experiment, we can determine the dominant resonance structures and realize the predominant nature of ICT within the molecule to a first-order approximation. Such analysis based on structural data is simple and intuitive, yet offers an effective method to understand certain electronic properties of molecules, e.g. their UV−vis absorption spectra. A comprehensive map of possible resonance states applicable to all coumarin laser dyes is illustrated in Figure 7, which helps to interpret the bond-length patterns in these molecules.

3.3. Propensity for *Para*-Quinoidal Resonance Structures in Laser Dye Coumarins. Electron-donating groups are attached at the 7-position and enhance the ICT from ring 1 to ring 2 in 29 subject coumarin laser dyes (**1**−**4** and **6**−**30**, Scheme 1). The net effect is the stabilization of *para*-quinoidal resonance structure **III** (Figure 7), since the 7-substitution extends the π-conjugated bonding through the *para*-quinoidal structure of ring 1 to the *para*-position (C4−C10). Accordingly, the bond-length patterns in ring 1 of these coumarins reflect this predominance of resonance state **III**. For example, C5−C6 and C8−C9 are the shortest bonds in ring 1 of **1**−**4** (Table 2). In fact, all coumarin laser dyes share the same pattern (Supporting Information).

Resonance structure **III** is also manifested by the characteristic partial double-bond nature of the C7−D (D═N or O) bond in the 7-position substituent. For example, this is illustrated via our crystal structural data for **1**−**4**, where D═N (Table 2). First, N1 is well-aligned with the ring 1 plane, deviating by less than 0.135 Å for **1**−**4**. Second, the C7−N1 bond lengths lie between those of pure single and double carbon−nitrogen bonds (Table 2), cf. 1.44 and 1.27 Å, respectively.[28] Lastly, the torsion angles involving C7−N1 also suggest partial sp^2 hybridization of the nitrogen atom and good alignment of the nitrogen lone pair with the π-system of ring 1: the total torsion angle, χ_N, in Table 2, denotes the absolute value of the difference between the two torsion angles along C7−N1. This angle represents the overall out-of-plane torsion angle of the two substituent branches attached to the N1 atom with respect to the ring 1 plane. It ranges from 0° for

dx.doi.org/10.1021/jp209925y |J. Phys. Chem. A 2012, 116, 727–737

perfect planar sp^2 to 60° for idealized tetrahedral sp^3 nitrogen hybridization.[28] In **1**−**4**, this angle is less than 30°; N1 is therefore more akin to sp^2 hybridization. The same C7−D partial double-bond character is observed for all 29 subject compounds (Supporting Information).

Resonance theory works equally well to explain the bond lengths in ring 2. Again, using **1**−**4** for illustration purposes, the competing contributions of resonance structures **II** and **IV**−**VI** (Figure 7) render C2−C3 and C4−C10 longer than C3−C4. Meanwhile, C2−C3 and C4−C10 are shorter than the average single-bond length between aromatic and sp^2 hybridized carbon atoms of 1.470 Å (Table 2 and Supporting Information).[29] This shortening can be explained by the competing influence of resonance structures **I** and **III**. Nevertheless, their contributions are relatively small and C2−C3 and C4−C10 are still more akin to a typical single bond, whereas C3−C4 is more representative of a double bond. For the same reason, the carbonyl bond (C2═O2, Table 2) is slightly longer than the average bond length of typical C═O bonds in esters with similar bond type geometries (1.199 Å),[29] as is evidenced by the combined contributions from its resonance states **I**, **III**, **V**, and **VI**. Likewise, similar trends are observed for **6**−**30** (Supporting Information).

Lastly, it should be pointed out that our structural data for **1**−**4** (Table 2) were collected at a range of temperatures (120−180 K). Temperature effects could in principle cause slight variations in apparent bond lengths, due to different degrees of thermal vibrations. In practice, there is no direct comparison between these bond lengths; and our primary interest is to investigate bond-length patterns. In spite of the temperature differences, these molecules display similar *para*-quinoidal bond-length patterns.

3.4. Quantifying the Relative Contribution of the *para*-Quinoidal Resonance States. The precise level of each possible relative contribution of different resonance states in ring 1 can be quantified by an empirical harmonic oscillator stabilization energy (HOSE) model.[25,26] HOSE describes the energy by which a molecule is more stable than its Kekulé structure. It is defined as

$$\mathrm{HOSE} = \frac{1}{2}\left[\sum_{r=1}^{n_1}(R_r' - R_o^s)^2 k_r' + \sum_{r=1}^{n_2}(R_r' - R_o^d)^2 k_r''\right] \quad (1)$$

where R_r' and R_r'' are actual π-bond lengths, R_o^s and R_o^d are reference single and double bond lengths, n_1 and n_2 are numbers of single and double bonds, and k_r' and k_r'' are force constants further defined below

$$k_r' = a + bR_r'; \quad k_r'' = a + bR_r'' \quad (2)$$

where R_r is the actual bond length, and a and b are constants derived based on experimental data. For carbon−carbon bonds, R_o^s 1.467 Å, R_o^d = 1.349 Å, $a = 44.39 \times 10^4$ Pa, and $b = -26.02 \times 10^4$ Pa.[26] The following equation can therefore be obtained after substituting constants and performing unit conversions:

$$\mathrm{HOSE} = 301.15\left[\sum_{r=1}^{n_1}(R_r' - 1.467)^2(44.39 - 26.02R_r') + \sum_{r=1}^{n_2}(R_r'' - 1.349)^2(44.39 - 26.02R_r'')\right] \quad (3)$$

In the above equation, the units of bond length and HOSE are Å and kJ/mol respectively.

The HOSE model can be extended to compute the relative contribution for each of the n resonance states in benzene derivatives.[25,26] For example, the ith resonance state has a contribution of

$$C_i = \frac{(\mathrm{HOSE}_i)^{-1}}{\sum_{j=1}^{N}(\mathrm{HOSE}_j)^{-1}} \quad (4)$$

The inverse empirical relationship between the HOSE value of the ith resonance state and its relative contribution indicates that the more stable resonance state has a larger contribution to the overall molecular structure.

Calculations of canonical structure contributions using the HOSE model have led to good credibility in the past.[30] Here we also make use of this model to assess the relative contribution of the *para*-quinoidal resonance structure of ring 1 in laser dye coumarins. In our calculation, the four possible resonance structures of ring 1 are taken into account. These are blue-highlighted in Figure 7 in coumarin canonical forms, **I**−**IV**, and are herein denoted by Q (*para*-quinoidal), OQ (*ortho*-quinoidal), K1 (Kekulé configuration 1), and K2 (Kekulé configuration 2).

The relative contributions of all four resonance states are presented in Table 3. Here the analysis is limited to the eight coumarins in the total subject data which possess substituents only at their 4- and 7-positions since this is the formation mechanism of the *para*-quinoidal structure: in order to form a *para*-quinoidal structure, an electron-donor and an acceptor group are typically attached to the *para*-positions of a benzene ring. In laser dye coumarins, an electron-donor group always sits at the 7-position. However, the corresponding *para*-position, the 10-position, is always connected to C4; otherwise, we would destroy the framework definition of coumarins. The *para* electron-acceptor strength is therefore adjusted indirectly by attaching different substituents to C4.

Table 3 demonstrates that the Q contribution (resonance state **III**) always dominates the overall structural form, with the exception of **16** where the 7-position donor strength is particularly low. By correlating the fractional Q contribution to the UV−vis peak absorption wavelengths for these compounds (Table 3 and Figures 7, structure **III**, and 8), a positive and approximately linear relationship is discovered, with a correlation coefficient of 0.9101 (Figure 8). In fact, if we remove the data of **15** and **17** as indicated by the purple circles in Figure 8, this coefficient tends toward perfect correlation to 0.9909. Specific examination of compounds **15** and **17** shows that such removal is justified owing to the $-N(C_2H_5)_2$ nature of the 7-substituent. In terms of structure, these two coumarins have nonplanar structures at the 7-position caused by the rotation and bending of ethyl chains; in contrast, the other coumarins (except for the disordered **18**) represented in Figure 8 possess very planar molecular structures at the 7-position. This structural difference implies that these two coumarins need to be considered separately from the others.

Regarding the fractional contributions of the other three canonical forms of ring 1 (OQ, K1, or K2), there is no evident relationship between them and the UV−vis peak absorption wavelength; indeed, the correlation coefficients for these eight 4,7-substituted coumarins are less than 0.8.

3.5. UV−Vis Peak Absorption Wavelength Shifts As a Function of Electron-Donor/Acceptor Strength in *para*-Quinoidal Coumarins. The positive correlation between the absorption wavelengths and Q contributions of coumarins can be

Table 3. UV−Vis Peak Absorption Wavelengths and the CSD Reference Codes of Coumarins with Substitutions at Only the 7- and/or 4-Positions

compound	$\lambda_{abs,peak}$ (nm)	CSD ref code	7-substitution	4-substitution	Q contribution	OQ contribution	K1 contribution	K2 contribution
16	325	MUMBEL01[31]	−OH	$-CH_3$	0.2525	0.2498	0.2816	0.2162
10	354	WIKDEZ[32]	$-NH_2$	$-CH_3$	0.2907	0.2390	0.2809	0.1894
11	366	ZENMAG[33]	$-N(CH_3)_2$	$-CH_3$	0.3081	0.2313	0.2621	0.1984
17	380	SUGGEG[34]	$-N(C_2H_5)_2$	−H	0.3359	0.2132	0.2593	0.1916
13	382	SOTHEO[35]	$-NH_2$	$-CF_3$	0.3286	0.2368	0.2472	0.1874
18	395	HURYEY[36]	$-NHC_2H_5$	$-CF_3$	0.3412	0.2141	0.2456	0.1991
14	396	VEJCIW[23]	$-N(CH_3)_2$	$-CF_3$	0.3536	0.2177	0.2559	0.1728
15	405	KUGWUE[37]	$-N(C_2H_5)_2$	$-CF_3$	0.3341	0.2139	0.2499	0.2021

This group of coumarins includes **10**, **11**, and **13**−**15**, as well as Coumarin 4 ($C_{10}H_8O_3$; **16**), Coumarin 466 ($C_{13}H_{15}NO_2$; **17**), and Coumarin 500 ($C_{12}H_{10}F_3NO_2$; **18**) (Scheme 1), for which accurate crystal structure data at room temperature are available in the CSD. Choosing only room temperature data minimizes possible bias from the temperature effects (in any event low temperature data are scarce), as quantitative evaluations on their bond lengths are performed on this set of coumarins. In addition, a single-point energy calculation reveals that VEJCIW has a slightly lower ground-state energy (−967.91 hartree) than that of VEJCIW01 (−967.87 hartree); that is, VEJCIW represents the most thermodynamically stable known crystal form of **14** and is therefore employed in the HOSE calculations. Moreover, in this table all UV−vis peak absorption wavelengths are obtained from ethanol solution to avoid potential bias from the solvent effects.

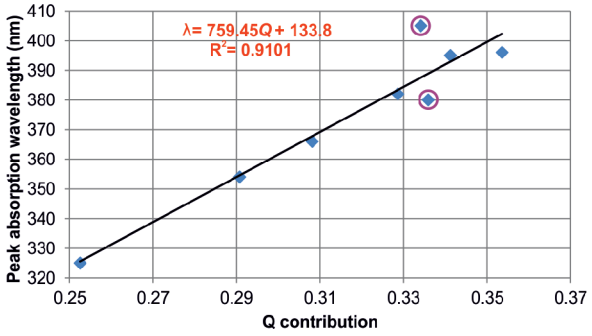

Figure 8. Correlation between UV−vis peak absorption wavelengths and the fractional Q contribution to the overall structure of ring 1 for the eight 4- and 7-substituted laser dye coumarins in this study. As their ring 1 becomes more *para*-quinoidal, these coumarins experience a red shift in UV−vis peak absorption wavelength. The two circled dots represent data of **15** and **17**, which have nonplanar substituent $-N(C_2H_5)_2$ located at their 7-position in contrast to other coumarins with (nearly) flat 7-substitution with respect to ring 1.

explored further by considering *para*-quinoidal coumarins with varying electron-donor/acceptor strengths. Photoexciting coumarin laser dyes induces ICT from ring 1 (donor) to ring 2 (acceptor). The ICT can be assisted by elevating the HOMO energy level of the donor in ring 1 and/or lowering the acceptor LUMO energy level in ring 2.[4] These changes in energy levels can be achieved by attaching different chemical substituents onto both rings. As the HOMO rises or the LUMO falls, the UV−vis absorption and emission wavelengths for these compounds experience a red shift, as less external energy is required to promote electrons from ring 1 to ring 2. Correspondingly, to tune such wavelengths toward their blue regime, electron-donating/-withdrawing substituents that widen the HOMO−LUMO energy difference (bandgap) should be employed. While the following illustration focuses on UV−vis peak absorption wavelengths, such conclusions can be equally extended to fluorescent and lasing wavelengths, since absorption, fluorescence and lasing all involve electron transitions between the S_0 and S_1 energy states of these molecules.

This influence of electron-donor/acceptor strength on the UV−vis spectral wavelength profile is exemplified via quantum-chemical calculations: ring 1 donor group effects are illustrated via three coumarins that have a common methyl group at their 4-position and a varying donor group at the 7-position, which takes the form $-NR_2$ (R = H or alkyl; Figure 9I). The ICT is pushed from ring 1 to ring 2, since $-NR_2$ is more electron-donating than the methyl group. In addition, the electron-donating strength of $-NR_2$ increases progressively from **10** to **12**. This is because alkyl groups donate charge to the nitrogen via inductive effects: the more branched, the greater this charge transfer; likewise, the greater the number of saturated bonds in the alkyl chain, the larger the charge polarization. This trend is reflected by the proliferating electron density in the HOMOs of the 7-position substituent from **10** to **12** (Figure 9IV). The charge is transferred from ring 1 to ring 2 upon photoexcitation, as indicated by the diminished electron density in the LUMOs of the 7-position substituents (Figure 9III). Furthermore, as the donor strength increases, the HOMO energy increases with respect to that of the LUMO, so causing the bandgap to shrink. Corresponding UV−vis peak absorption wavelengths experience a red shift in the order **10** < **11** < **12** (Figure 9II).

The effects of the electron-acceptor group in ring 2 are demonstrated by replacing the methyl group at the 4-position in the previous example for the highly electron-withdrawing trifluoromethyl group (Figure 10): this induces a much stronger "push-pull" effect from the donor group in ring 1 to the acceptor group in ring 2. Correspondingly, the UV−vis absorption wavelengths of the coumarins in this group show a larger red shift compared to their counterparts in Figure 9.

The aforementioned correlation between the level of red shift in UV−vis peak absorption wavelengths and the Q contribution (Figure 8) is therefore rationalized by inspection of the varying electron-donor/acceptor strength of the 4,7-disubstitution (Table 3).

3.6. UV−Vis Peak Absorption Wavelength Shifts As a Function of Varying Sites of Chemical Substitution. The relationship between the Q contribution and the UV−vis peak

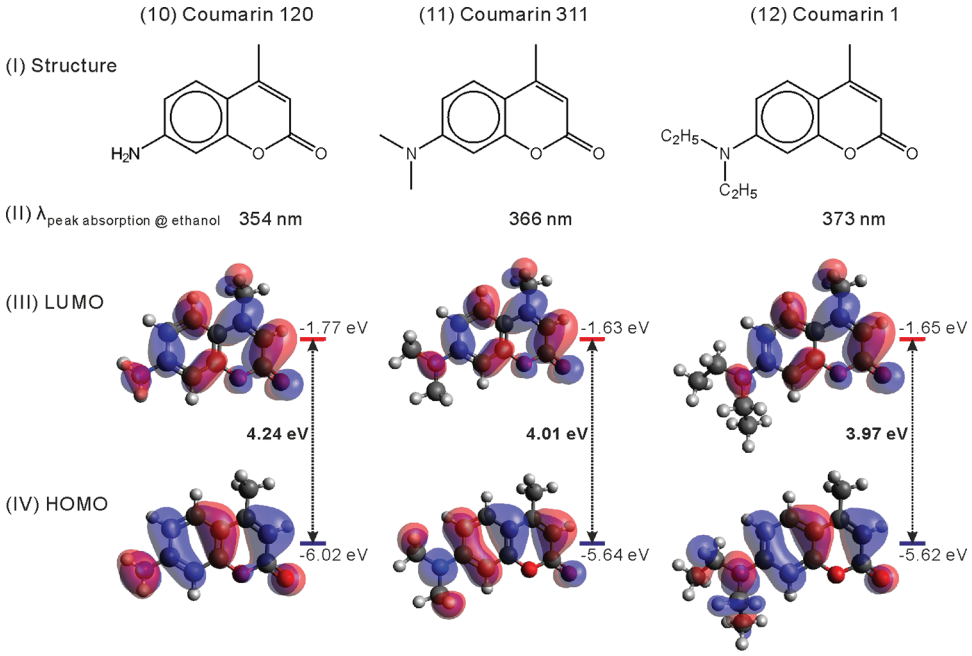

Figure 9. Coumarins with a common methyl group at the 4-position. (I) Their molecular structures and (II) UV−vis peak absorption wavelengths as measured in ethanol solution. (III) HOMO, (IV) LUMO (Red, positive; blue, negative; isovalue, 0.02), and the corresponding bandgaps of these molecules as computed in the gas phase.

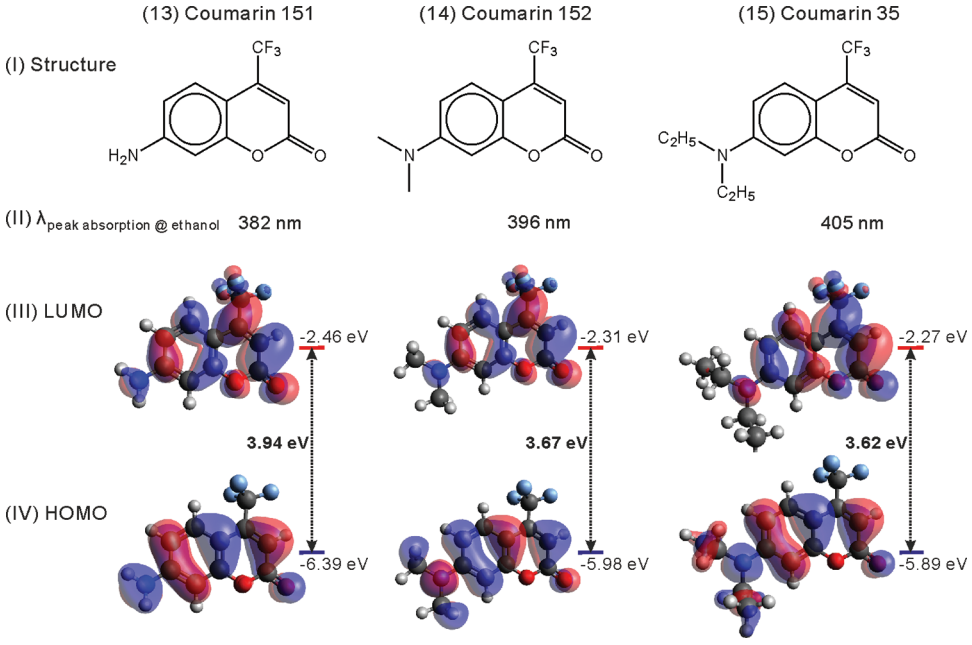

Figure 10. Coumarins with a common trifluoromethyl group at the 4-position. (I) Their molecular structures and (II) UV−vis peak absorption wavelengths as measured in ethanol solution. (III) HOMO, (IV) LUMO (Red, positive; blue, negative; isovalue, 0.02) and the corresponding bandgaps of these molecules as computed in the gas phase. Note that their bandgaps are smaller compared to their 4-methyl analogues in Figure 9.

absorption wavelengths of laser dyes is more difficult to quantify when chemical substituents are attached to other positions in the coumarin framework. However, although such quantification cannot be described as a linear relationship, in contrast to 4, 7-substituted coumarins (Figure 8), there remains a distinct and strong positive correlation (Figure 11). Attaching an electron-withdrawing group at the 3-position clearly affords a larger red shift in the UV−vis absorption spectrum and a stronger *para*-quinoidal bond length character than if it were on the 4-position.

This stands to reason since an electron-withdrawing group at the 3-position will remove electron density from the formal C3═C4 double bond, thereby favoring resonance state **III** (Figure 7): hence, a higher Q contribution. The effectiveness of electron-withdrawing substituents at the 3-position can also be explained via the direction of charge transfer within coumarins.

dx.doi.org/10.1021/jp209925y |*J. Phys. Chem. A* 2012, 116, 727–737

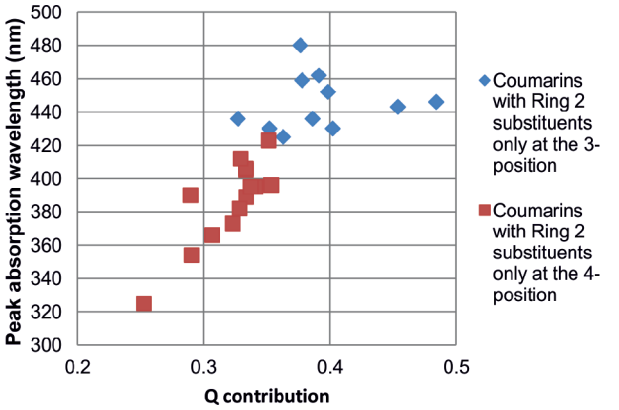

Figure 11. UV−vis peak absorption wavelengths and Q contributions of coumarins with ring 2 substituents only at the 3- or 4-positions. Generally speaking, there is a positive correlation between Q contribution and UV−vis peak absorption wavelength. When a substituent is attached to the 3- instead of the 4-position, a larger spectral red shift and a higher Q contribution are observed, due to more effective assistance to the ICT.

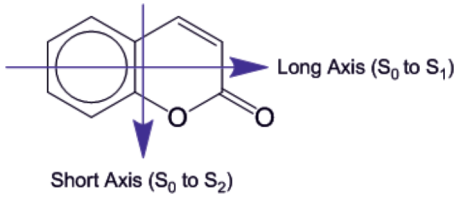

Figure 12. Charge transfer directions in coumarins. The long axis charge transfer corresponds to a lower energy jump and any chemical substituent contributing to this direction of charge transfer produces a bigger impact on wavelength shifts in coumarin laser dyes.

ICT can occur either along the long or the short axes of a molecule with pseudoreflective symmetry.[38] In coumarins, electron transfer along the long axis corresponds to a low energy jump (S_0 to S_1) compared to that of the short axis (S_0 to S_2) (Figure 12).[38] Consequently, light absorption and emission spectra are mainly determined by the long axis charge transfer, and substituents attached along this direction play a more noteworthy role than those attached along the short axis.[38] The attachment of electron-withdrawing groups in the 3-position aligns more closely to the long axis and thus produces a greater impact on spectral shift.

3.7. Effect of Chemical Substitution Site Variation on the Molar Extinction Coefficient. The addition of electron-withdrawing substituents at the 3-position not only leads to a large red shift in coumarin UV−vis absorption spectra but it also increases the light absorption efficiency of coumarins, owing to the facilitation of ICT. These light absorption efficiencies are quantified by the molar extinction coefficient ε, a parameter used to describe how strongly a material absorbs light per molar concentration. Note that a high molar extinction coefficient is a very important criterion for high-efficiency DSC dyes, especially when a cosensitization strategy is adopted.[39]

Large ε values are observed in coumarins with ring 2 substituents at the 3-position (Figure 13). Here, 23 ε values are divided into two groups (red and green) representing coumarins with ring 2 chemical substitution at their 4- or 3-positions, respectively. The extinction coefficients of the majority of coumarins in

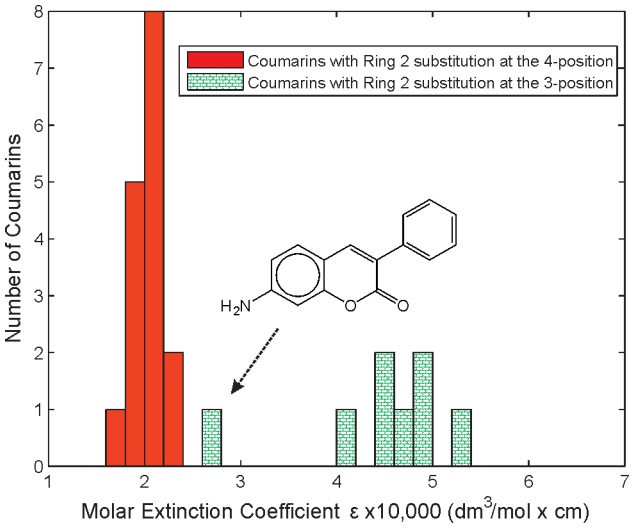

Figure 13. Histogram of the molar extinction coefficients (ε) of coumarins. The ε values of coumarins with ring 2 substituents at the 3-position are approximately twice as large as those with the 4-position substituents. The relatively low ε value of **5** as shown in this figure is caused by the weak electron-withdrawing strength of the phenyl ring.

the 3-substituted group are approximately twice as large as those of the 4-substituted group. Moreover, even the lowest ε value with 3-substitution (in ring 2) from Coumarin 10 ($C_{15}H_{11}NO_2$; **5**) is still approximately 15% larger than the highest ε value with 4-substitution (in ring 2).

Indeed, the relatively low extinction coefficient of **5** can be explained by its molecular structure. The substituent on the 3-position in **5** is a phenyl ring. Terminal phenyl rings have negligible charge transfer properties, as indicated by their near zero Hammett values.[40] Such weak donating/withdrawing strength results in a feeble "push-pull" effect on the ICT, thereby accounting for the relatively small extinction coefficient of **5**.

Nevertheless, in general, coumarins with substituents on the 3-position possess high molar extinction coefficients, and it seems that this chemical substitution positional effect has a disproportionately large effect on ε compared with the effect of varying the electron-donating/-withdrawing strengths of the substituents. For example, the $-CF_3$ group, a common chemical substituent at the 4-position, has a slightly higher electron-withdrawing strength than those of $-COOH$, $-COOCH_3$, and $-COOC_2H_5$, as indicated by their respective Hammett values.[40] Yet, by attaching one of these three substituents to the 3-position, to yield Coumarin 334 ($C_{17}H_{17}NO_3$; **7**), Coumarin 343 ($C_{16}H_{15}NO_4$; **8**), and Coumarin 314 ($C_{18}H_{19}NO_4$; **9**) respectively, we observe an approximately 2-fold increase in ε values compared to Coumarin 153 ($C_{16}H_{14}F_3NO_2$; **6**) with $-CF_3$ at the 4-position: $\varepsilon = 2.0 \times 10^4$ dm^3 mol^{-1} cm^{-1} **6**, 4.9×10^4 dm^3 mol^{-1} cm^{-1} **7**, 4.43 × dm^3 mol^{-1} cm^{-1} **8**, 4.68×10^4 dm^3 mol^{-1} cm^{-1} **9** (Supporting Information).

4. CONCLUDING REMARKS

In this paper, the molecular structures of various coumarin derivatives used in dye laser applications have been studied. A common feature of these coumarins is that one electron-donating group (typically an amine group) is attached at the 7-position of the coumarin framework; another electron-withdrawing group is sometimes attached at the 3- or 4-position.

Intramolecular charge transfer occurs due to a "push-pull" effect which leads to a predominance of *para*-quinoidal resonance states in the benzene rings of these coumarins. Correspondingly, C5−C6 and C8−C9 bonds are relatively short. By using the HOSE model, the contribution of the *para*-quinoidal state (Q contribution) is quantified. We find a linear correlation between this Q contribution and the UV−vis peak absorption wavelengths of coumarins where substituents lie only at the 4- and 7-positions. It is shown that this can be rationalized by relative "push-pull" effects caused by attaching various electron-donating/-withdrawing substituents to ring 1/ring 2. Increasing the "push-pull" effect reduces coumarin bandgaps and leads to a spectral red shift in UV−vis absorption; this conclusion is supported by quantum-chemical calculations. Lastly, it is noted that attaching electron-withdrawing groups to the 3-position instead of the 4-position affords greater spectral red shifts and higher molar extinction coefficients.

The overarching reason for carrying out these structure−property relationship studies on coumarins is to understand their electronic operational mechanisms such that one can begin to rationally design more efficient coumarin dyes for laser and DSC applications. Understanding the "push-pull" effect on the ICT, wavelength tuning and molar extinction coefficient enhancement provides an important foundation for the ultimate ability to molecular engineer "dial-up" optoelectronic properties to suit a given device application.

■ ASSOCIATED CONTENT

Supporting Information. Tables of coumarin laser dyes with their CSD reference codes, bond lengths, spectral information, and molar extinction coefficients, as well as crystallographic information files (CIFs) for **1**−**4**. This material is available free of charge via the Internet at http://pubs.acs.org.

■ AUTHOR INFORMATION

Corresponding Author

*E-mail: jmc61@cam.ac.uk.

Present Addresses

⊥Department of Physics, University of Bath, Bath, BA2 7AY United Kingdom.

■ ACKNOWLEDGMENT

X.L. is indebted to the Singapore Economic Development Board for a Clean Energy Scholarship. J.M.C. thanks the Royal Society for a University Research Fellowship, the University of New Brunswick (UNB) for The UNB Vice-Chancellor's Research Chair and NSERC for the Discovery Grant, 355708 (for P.G.W.). T.C.L. is indebted to the Taiwanese Ministry of Education for a partially funded Ph.D. studentship. J.R. acknowledges the EPSRC for a DTA Ph.D. studentship (EP/P505445/1). ACEnet, the regional high performance computing consortium for universities in Atlantic Canada, is acknowledged for providing computational facilities for this work. The authors also thank Drs. Shamus Husheer and Staffan Wallin, formerly from the University of Cambridge for their assistance in X-ray diffraction.

■ REFERENCES

(1) Kontogiorgis, C.; Hadjipavlou-Litina, D. *J. Enzym. Inhib. Med. Ch.* **2003**, *18*, 63–69.
(2) Zhao, H.; Neamati, N.; Hong, H.; Mazumder, A; Wang, S.; Sunder, S.; Milne, G. W.; Pommier, Y.; Burke, T. R. *J. Med. Chem.* **1997**, *40*, 242–249.
(3) Deng, R. W.; Wu, J. G.; Long, L. S. *B. Soc. Chim. Belg.* **1992**, *101*, 439–443.
(4) Duarte, F. J.; Hillman, L. W. *Dye Laser Principles, with Applications*; Academic Press Inc.: San Diego, CA, 1990.
(5) Hara, K.; Kurashige, M.; Dan-oh, Y.; Kasada, C.; Shinpo, A.; Suga, S.; Sayama, K.; Arakawa, H. *New J. Chem.* **2003**, *27*, 783–785.
(6) Mishra, A.; Fischer, M. K. R.; Bäuerle, P. *Angew. Chem., Int. Ed.* **2009**, *48*, 2474–2499.
(7) Allen, F. H. *Acta Crystallogr., Sect. B: Struct. Sci.* **2002**, *58*, 380–388.
(8) Ueno, K. *Acta Crystallogr., Sect. C: Cryst. Struct. Commun.* **1985**, *41*, 1786–1789.
(9) *CrystalClear-SM Expert and CrystalStructure*; Rigaku: Woodlands, Texas, 2009.
(10) *COLLECT, data collection software*; Nonius: Delft, Netherlands, 1998.
(11) Otwinowski, Z.; Minor, W. *Method. Enzymol.* **1997**, *276*, 307–326.
(12) Blessing, R. H. *J. Appl. Crystallogr.* **1997**, *30*, 421–426.
(13) Sheldrick, G. M. *Acta Crystallogr., Sect. A: Found. Crystallogr.* **2008**, *64*, 112–122.
(14) Farrugia, L. J. *J. Appl. Crystallogr.* **1997**, *30*, 565.
(15) Westrip, S. P. *J. Appl. Crystallogr.* **2010**, *43*, 920–925.
(16) Reynolds, G. A.; Drexhage, K. H. *Opt. Commun.* **1975**, *13*, 222–225.
(17) Fletcher, A. N.; Bliss, D. E. *Appl. Phys.* **1978**, *16*, 289–295.
(18) Frisch, M. J.; Trucks, G. W.; Schlegel, H. B.; Scuseria, G. E.; Robb, M. A.; Cheeseman, J. R.; Scalmani, G.; Barone, V.; Mennucci, B.; Petersson, G. A.; Nakatsuji, H.; Caricato, M.; Li, X.; Hratchian, H. P.; Izmaylov, A. F.; Bloino, J.; Zheng, G.; Sonnenberg, J. L.; Hada, M.; Ehara, M.; Toyota, K.; Fukuda, R.; Hasegawa, J.; Ishida, M.; Nakajima, T.; Honda, Y.; Kitao, O.; Nakai, H.; Vreven, T.; Montgomery, Jr., J. A.; Peralta, J. E.; Ogliaro, F.; Bearpark, M.; Heyd, J. J.; Brothers, E.; Kudin, K. N.; Staroverov, V. N.; Kobayashi, R.; Normand, J.; Raghavachari, K.; Rendell, A.; Burant, J. C.; Iyengar, S. S.; Tomasi, J.; Cossi, M.; Rega, N.; Millam, N. J.; Klene, M.; Knox, J. E.; Cross, J. B.; Bakken, V.; Adamo, C.; Jaramillo, J.; Gomperts, R.; Stratmann, R. E.; Yazyev, O.; Austin, A. J.; Cammi, R.; Pomelli, C.; Ochterski, J. W.; Martin, R. L.; Morokuma, K.; Zakrzewski, V. G.; Voth, G. A.; Salvador, P.; Dannenberg, J. J.; Dapprich, S.; Daniels, A. D.; Farkas, Ö.; Foresman, J. B.; Ortiz, J. V.; Cioslowski, J.; Fox, D. J. *Gaussian 09*, revision A.1; Gaussian Inc.: Wallingford, CT, 2009.
(19) Lee, C.; Yang, W.; Parr, R. G. *Phys. Rev. B* **1988**, *37*, 785–789.
(20) Becke, A. D. *J. Chem. Phys.* **1993**, *98*, 5648–5652.
(21) Stephens, P. J.; Devlin, F. J.; Chabalowski, C. F.; Frisch, M. J. *J. Phys. Chem.* **1994**, *98*, 11623–11627.
(22) Rassolov, V. A.; Ratner, M. A.; Pople, J. A.; Redfern, P. C.; Curtiss, L. A. *J. Comput. Chem.* **2001**, *22*, 976–984.
(23) Chinnakali, K.; Sivakumar, K.; Natarajan, S. *Acta Crystallogr., Sect. C: Cryst. Struct. Commun.* **1990**, *46*, 833–835.
(24) Jasinski, J. P.; Paight, E. S. *Acta Crystallogr., Sect. C: Cryst. Struct. Commun.* **1994**, *50*, 1928–1930.
(25) Oziminski, W. P.; Krygowski, T. M. *J. Phys. Org. Chem.* **2010**, *23*, 551–556.
(26) Krygowski, T. M.; Anulewicz, R.; Kruszewski, J. *Acta Crystallogr., Sect. B: Struct. Sci.* **1983**, *39*, 732–739.
(27) Liu, X.; Cole, J. M.; Waddell, P. G.; Lin, T.-C. *Acta Crystallogr., Sect. B: Struct. Sci.* **2011**, *67*, 560–568.
(28) Gilli, G.; Bertolasi, V.; Bellucci, F.; Ferretti, V. *J. Am. Chem. Soc.* **1986**, *108*, 2420–2424.
(29) Allen, F. H.; Kennard, O.; Watson, D. G.; Brammer, L.; Orpen, A. G.; Taylor, R. *J. Chem. Soc. Perkin Trans. 2* **1987**, S1–S19.
(30) Krygowski, T. M.; Cyranski, M. K. *Synlett* **2003**, *7*, 922–936.
(31) Yang, S.-P.; Han, L.-J.; Wang, D.-Q.; Xia, H.-T. *Acta Crystallogr., Sect. E: Struct. Rep. Online* **2007**, *63*, o4643.
(32) Jasinski, J. P.; Woudenberg, R. C. *Acta Crystallogr., Sect. C: Cryst. Struct. Commun.* **1994**, *50*, 1954–1956.

(33) Yip, B.-C.; Yaw, O.-L.; Ong, L.-H.; Fun, H.-K.; Sivakumar, K. *Acta Crystallogr., Sect. C: Cryst. Struct. Commun.* **1995**, *51*, 2087–2089.
(34) Yufit, D. S.; Kirpichenok, M. A.; Struchkov, Y. T.; Karandashova, L. A.; Grandberg, I. I. *Izv. Akad. Nauk SSSR, Ser. Khim (Russ. Chem. Bull.)* **1991**, *40*, 702–710.
(35) Selladurai, S.; Subramanian, K. *Acta Crystallogr., Sect. C: Cryst. Struct. Commun.* **1992**, *48*, 281–283.
(36) Jasinski, J. P.; Jasinski, J. M.; Li, Y.; Crosby, D. J. *Acta Crystallogr., Sect. E: Struct. Rep. Online* **2003**, *59*, o153–o154.
(37) Chinnakali, K.; Sivakumar, K.; Natarajan, S. *Acta Crystallogr., Sect. C: Cryst. Struct. Commun.* **1992**, *48*, 1859–1862.
(38) Pavlopoulos, T. G. *IEEE J. Quantum Elect.* **1973**, *QE-9*, 510–516.
(39) Robertson, N. *Angew. Chem., Int. Ed.* **2008**, *47*, 1012–1014.
(40) Dean, J. A. *Lange's Handbook of Chemistry*; McGraw-Hill: New York, 1999.